Research Article | Vol. 24, No. 21 | 17 Oct 2016 | OPTICS EXPRESS 24265

Optics EXPRESS

Electrically switchable diffractive waveplates with metasurface aligned liquid crystals

JEFFREY CHOU,[1,*] LALITHA PARAMESWARAN,[1] BRIAN KIMBALL,[2] AND MORDECHAI ROTHSCHILD[1]

[1]*Lincoln Laboratory, Massachusetts Institute of Technology, Lexington, MA 02420, USA*
[2]*U.S. Army Natick Soldier Research, Development and Engineering Center, Natick, MA 01760, USA*
**jeff.chou@ll.mit.edu*

Abstract: Diffractive waveplates and equivalent metasurfaces provide a promising path for applications in thin film beam steering, tunable lenses, and polarization filters. However, fixed metasurfaces alone are unable to be tuned electronically. By combining metasurfaces with tunable liquid crystals, we experimentally demonstrate a single layer device capable of electrically switching a diffractive waveplate design at a measured peak diffraction efficiency of 35%, and a minimum switching voltage of 10V. Furthermore, the nano-scale metasurface aligned liquid crystals are largely independent of variations in wavelength and temperature. We also present a computational analysis of the efficiency limits of liquid crystal based diffractive waveplates, and compare this analysis to experimental measurements.

OCIS codes: (050.1950) Diffraction gratings; (130.4815) Optical switching devices; (160.3710) Liquid crystals.

References and links

1. S. V. Serak, R. S. Hakobyan, S. R. Nersisyan, N. V. Tabiryan, T. J. White, T. J. Bunning, D. M. Steeves, and B. R. Kimball, "All-optical diffractive/transmissive switch based on coupled cycloidal diffractive waveplates," Opt. Express **20**(5), 5460–5469 (2012).
2. S. R. Nersisyan, N. V. Tabiryan, L. Hoke, D. M. Steeves, and B. R. Kimball, "Polarization insensitive imaging through polarization gratings," Opt. Express **17**(3), 1817–1830 (2009).
3. G. Li, D. L. Mathine, P. Valley, P. Ayräs, J. N. Haddock, M. S. Giridhar, G. Williby, J. Schwiegerling, G. R. Meredith, B. Kippelen, S. Honkanen, and N. Peyghambarian, "Switchable electro-optic diffractive lens with high efficiency for ophthalmic applications," Proc. Natl. Acad. Sci. U.S.A. **103**(16), 6100–6104 (2006).
4. N. V. Tabiryan, S. V. Serak, D. E. Roberts, D. M. Steeves, and B. R. Kimball, "Thin waveplate lenses of switchable focal length--new generation in optics," Opt. Express **23**(20), 25783–25794 (2015).
5. C. Maurer, A. Jesacher, S. Fürhapter, S. Bernet, and M. Ritsch-Marte, "Tailoring of arbitrary optical vector beams," New J. Phys. **9**(3), 78 (2007).
6. G. Li, P. Valley, M. S. Giridhar, D. L. Mathine, G. Meredith, J. N. Haddock, B. Kippelen, and N. Peyghambarian, "Large-aperture switchable thin diffractive lens with interleaved electrode patterns," Appl. Phys. Lett. **89**(14), 141120 (2006).
7. L. Li, D. Bryant, T. Van Heugten, and P. J. Bos, "Near-diffraction-limited and low-haze electro-optical tunable liquid crystal lens with floating electrodes," Opt. Express **21**(7), 8371–8381 (2013).
8. S. Nersisyan, N. Tabiryan, D. M. Steeves, and B. R. Kimball, "Fabrication of liquid crystal polymer axial waveplates for UV-IR wavelengths," Opt. Express **17**(14), 11926–11934 (2009).
9. D. Lin, P. Fan, E. Hasman, and M. L. Brongersma, "Dielectric gradient metasurface optical elements," Science **345**(6194), 298–302 (2014).
10. M. Khorasaninejad, W. T. Chen, R. C. Devlin, J. Oh, A. Y. Zhu, and F. Capasso, "Metalenses at visible wavelengths: Diffraction-limited focusing and subwavelength resolution imaging," Science **352**(6290), 1190–1194 (2016).
11. E. Arbabi, A. Arbabi, S. M. Kamali, Y. Horie, and A. Faraon, "Multiwavelength polarization-insensitive lenses based on dielectric metasurfaces with meta-molecules," Optica **3**(6), 628–633 (2016).
12. H. Sarkissian, J. B. Park, B. Y. Zeldovich, and N. V. Tabirian, "Periodically aligned liquid crystal: potential application for projection displays," ArXivcond-Mat0508555 (2005).
13. L. Tan, J. Y. Ho, and H.-S. Kwok, "Extended Jones matrix method for oblique incidence study of polarization gratings," Appl. Phys. Lett. **101**(5), 051107 (2012).
14. P. Yeh, "Extended Jones matrix method," J. Opt. Soc. Am. **72**(4), 507 (1982).
15. H. H. Cheng, A. K. Bhowmik, and P. J. Bos, "Concept for a transmissive, large angle, light steering device with high efficiency," Opt. Lett. **40**(9), 2080–2083 (2015).
16. C. Oh and M. J. Escuti, "Achromatic diffraction from polarization gratings with high efficiency," Opt. Lett. **33**(20), 2287–2289 (2008).

#273488 http://dx.doi.org/10.1364/OE.24.024265
Journal © 2016 Received 9 Aug 2016; revised 29 Sep 2016; accepted 1 Oct 2016; published 11 Oct 2016

Optics EXPRESS

17. S. A. Vitale and S. Berry, "Etching selectivity of indium tin oxide to photoresist in high density chlorine- and ethylene-containing plasmas," J. Vac. Sci. Technol. B **31**(2), 021210 (2013).
18. I. Chuang, R. Durrer, N. Turok, and B. Yurke, "Cosmology in the Laboratory: Defect Dynamics in Liquid Crystals," Science **251**(4999), 1336–1342 (1991).
19. N. I. Zheludev and Y. S. Kivshar, "From metamaterials to metadevices," Nat. Mater. **11**(11), 917–924 (2012).

1. Introduction

Diffractive waveplates (DW) offer extremely high diffraction efficiencies by utilizing a liquid crystal layer only microns thick [1]. Furthermore, under the correct configuration, full electronic tunability may also be accomplished to allow for optoelectronic, thin film beam steering, tunable lenses, beam shaping, and polarization filters [1–7]. The potential impact of diffractive waveplates can revolutionize electro-optical applications that require low size, weight, and power. Various diffractive waveplate designs have been previously demonstrated such as the cycloidal diffractive waveplate (CDW), also known as the Pancharatnam phase device, which can be used for beam steering and polarization sensing [1]. Axial wave plates (AWP) have been developed to control beam shapes and generate highly ordered "doughnut" beams for applications in imaging, spectral filtering, and optical tweezers [5,8]. Recently all dielectric metasurfaces have also been demonstrated as highly efficiency flat lenses and polarization filters, however, these devices remain fixed and are unable to be tuned electronically [9–11]. We note the operating principal behind the dielectric metasurfaces and DWs are similar in that they both rely on subwavelength polarization rotations via half-wave plates [10]. The aim of this work is to study electrically tunable metasurface designs using liquid crystals as the enabling material.

Current fabrication methods for DWs typically employ interference lithography to generate periodic polarization patterns on photoalignment surfaces [1]. These surfaces are used to align layer for birefringent liquid crystal layers up to a thickness equal to the half wave condition. Despite the ability to pattern large areas using interference lithography on photoalignment layers, two main hurdles remain: 1) inability to pattern arbitrary patterns, and 2) limited reliability across all wavelengths and under long exposure times. The first issue is inherent to the periodic nature of interference lithography. Direct write optical methods based on mechanically raster-scanning polarized light do allow for arbitrary patterns on photoalignment layers, but reliability issues remain [8]. The second issue is due to the fundamental nature of photoalignment surfaces, where high energy light, prolonged exposure to broadband light (*e.g.*, sunlight), or high temperatures can spoil the patterned surface. Arbitrary patterning of DW can be useful when combining variably pitched patterns, integrating with electrodes, or creating more complex designs.

In this paper we describe a method that employs electron-beam patterned etched surfaces to create complex DW metasurface designs using switchable liquid crystals. The etched surfaces create a wavelength and temperature robust alignment surface for the liquid crystals and also enable arbitrary patterns. Here we present the theory, performance limits, fabrication, and characterization of a robust etched CDW device.

2. Theory

The CDW is composed of a nematic liquid crystal layer in which the azimuth of the director n rotates monotonically along the in-plane x-direction with a period a, as shown in Fig. 1(a). The orientation of the liquid crystal extends throughout the thickness of the liquid crystal cell, t, as shown in Fig. 1(b). The ideal thickness, t, for a CDW is defined by the half-wave condition in Eq. (1)

$$t = \frac{\lambda}{2\Delta n} \tag{1}$$

Optics EXPRESS

where t is the thickness of the liquid crystal cell, λ is the wavelength, and Δn is the index contrast of the birefringent liquid crystal. When non-polarized light is incident along the z-axis of the CDW, the transmitted light is diffracted into only the M_{+1} and M_{-1} modes. The zeroth order M_0 mode is eliminated due to destructive interference. If the incident light is circularly polarized, only one of the diffracted modes will transmit, as shown in Fig. 1(c). More precise mathematical descriptions of the physical behavior behind CDWs have been published previously [12–14]. In a real system, reflections due to glass surfaces should also be taken into account. Anti-reflection layers can be used to mitigate these effects.

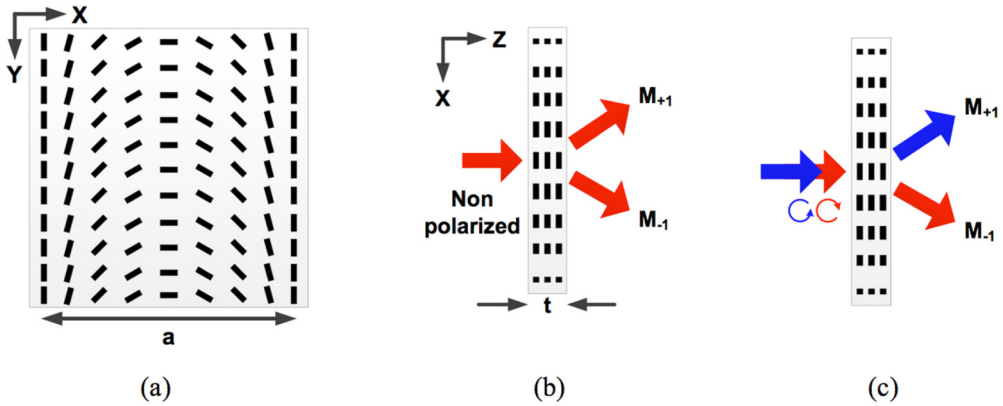

Fig. 1. (a) Shows the schematic of the rotation orientation of the liquid crystal direction. The ideal operation of the CDW is shown with non-polarized (b) and circularly polarized (c) inputs.

In order to understand the performance limits of a CDW, we define efficiency metrics to analyze both the diffraction efficiency and polarization efficiency. In a non-ideal CDW cell, the M_0 mode intensity is not completely suppressed, and contains a measurable value, as shown in Fig. 2 (a). The metric for the diffraction efficiency (DE) is defined in the equation shown in Fig. 2(b), where an ideal CDW possesses a DE = 1. In this expression it is assumed that the diffraction into the M_{+1} and M_{-1} modes is the same, and DE is a measure of the effectiveness of the CDW to suppress M_0. The second metric is defined as the polarization efficiency (PE). In a non-ideal CDW, when a circularly polarized input is incident on the CDW, the transmitted non-desired M_{+1} and M_0 mode may still contain a measurable value, as shown in Fig. 2(c). The metric definition for PE is shown in Fig. 2(d), where the ideal CDW possess a PE = 1. The expression in 2(d) neglects any transmitted power in M_0 in order to isolate the polarization filtering efficiency.

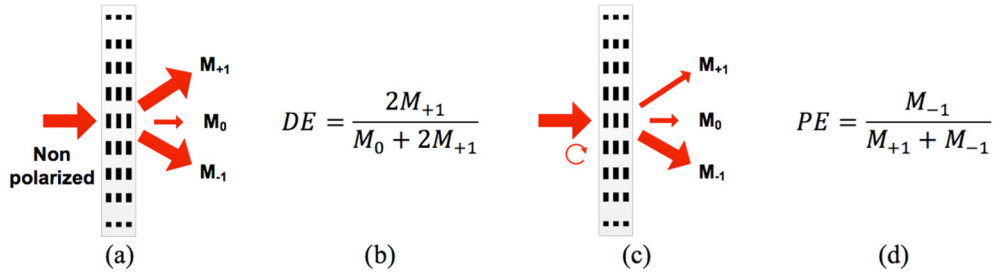

Fig. 2. Metric definitions for diffraction efficiency (a), (b), and polarization efficiency (c), (d).

One of the key questions for diffractive waveplates in general is: what is the maximum diffraction angle achievable for a given target efficiency? Understanding this limit will help set the spatial-frequency requirements of more advanced and arbitrary designs. The ideal

Optics EXPRESS

operation of the CDW is an infinitely thin half-wave plate, where the polarization of the incident light is instantaneously rotated at the CDW interface. With such an ideal device, extremely large diffraction angles could be achieved theoretically. Unfortunately, in real devices the liquid crystal thickness is defined by the half-wave condition of Eq. (1). Intuitively, when diffracted light propagates through the finite-thickness LC cell at large angles, the light traverses through the off-axis CDW index profile accruing non-ideal phase. As a result, the non-ideal phase accumulation prevents ideal deconstructive interference of the M_0 mode. A previous report has theoretically demonstrated large diffraction angles by utilizing a dual layer double twist CDW device, although experimentally creating such a device remains a challenge [15,16].

Based on Eq. (1), the best method to reduce the liquid crystal cell thickness is to increase the Δn of the liquid crystal. However, in practice the range of options is quite limited. Typical liquid crystals, such as 5CB, possess a $\Delta n \approx 0.15$ in the visible spectrum, while more exotic liquid crystals possess a $\Delta n \approx 0.25$ at most.

In order to quantitatively demonstrate this effect, we use finite-difference time-domain (FDTD) simulations. The FDTD simulation included only the liquid crystal cell with no glass enclosure. The liquid crystal itself was modeled with a wavelength independent index contrast Δn. The etched ITO structure was not included in the simulations, as our goal was to simulate the CDW under the most ideal conditions. Periodic Bloch boundary conditions were used. The contour map in Fig. 3(a) shows the simulated DE for various Δn and diffraction angles at a wavelength of 405 nm. The diffraction angle is determined by the period of the CDW pattern. For example, with a $\Delta n = 0.15$ and a DE = 0.9, the maximum M_{+1} diffraction angle is 17°. From the simulation we see that higher diffraction angles for a given Δn can be achieved but at the expense of efficiency. We can also confirm our previous conclusion that the maximum diffraction angle improves with increasing Δn, due to the reduced thickness of the LC cell. The efficiency for a given Δn decreases with increasing wavelength, as seen in Fig. 3(b), where the DE simulation was repeated at a wavelength of 600 nm. For example, at $\Delta n = 0.15$, the diffraction angle at DE = 0.9 decreases from 17° to 13° when increasing the wavelength from 405 nm to 600 nm. The results from these simulations define the spatial-frequency limit of advanced liquid crystal diffractive waveplates.

The PE analysis of the CDW was also performed via FDTD simulation, but yielded no dependency on diffraction angle or Δn. This result implies that the off-axis propagation of diffracted light through a finite thickness liquid crystal cell only contributes to the M_0 mode, and does not contribute to the oppositely diffracted mode.

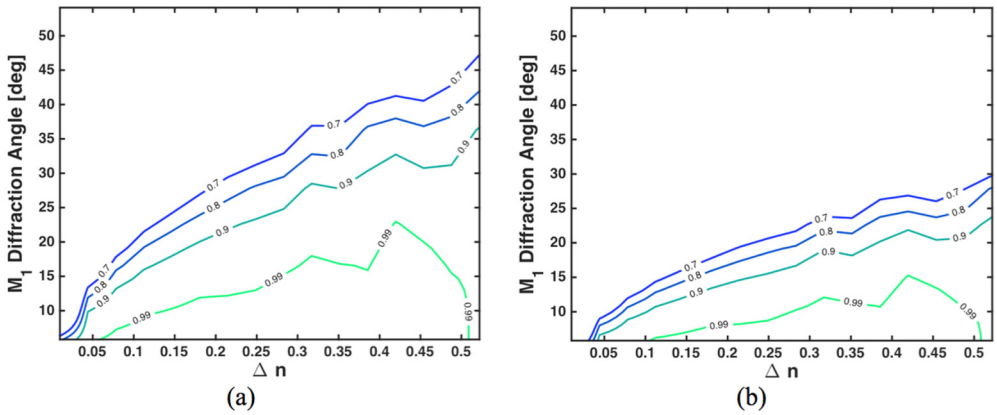

Fig. 3. FDTD simulated DE for a CDW liquid crystal cell with a thickness equal to the half-wave condition at wavelengths of (a) 405 nm and (b) 600 nm. The DE values are labeled in line as a function of both the M_1 diffraction angle and the liquid crystal Δn.

Optics EXPRESS

3. Experimental results

The fabrication process flow in Fig. 4 shows the indium tin oxide (ITO) etched CDW chip fabricated at MIT Lincoln Laboratory. The 400-nm-thick ITO is deposited on a BK-7 glass substrate via sputtering, followed by a deposition of a dual-layer PMMA resist step. After patterning of the PMMA with a 100kV Vistec scanning electron beam lithography system, 80 nm of nickel is electron-beam evaporated and lifted off to create a hardmask for reactive ion etching (RIE) of the ITO. The RIE of ITO is performed in an inductively coupled plasma etcher, with a chlorine chemistry which has a high selectivity with respect to nickel [17]. Following the RIE of ITO, the nickel hardmask is chemically stripped in Transene nickel etchant. The full liquid crystal cell is formed by attaching a second ITO-on-glass substrate separated by a photolithographically defined photoresist spacer layer. AZ1512 cross-linkable photoresist is used as the spacer layer in order to precisely define the liquid crystal cell thickness and bring it as close as possible to the half-wave condition for a 405 nm wavelength laser (~1.2 μm). The photoresist was then hardbaked for 15 minutes at 125°C. The liquid crystals used in these experiments were either 5CB from Sigma-Aldrich or 6CHBT from Beam Co. The 6CHBT liquid crystal has a Δn = 0.17 at a wavelength of 633 nm. The liquid crystal was pipetted onto the etched glass disc before the second top glass disc was applied.

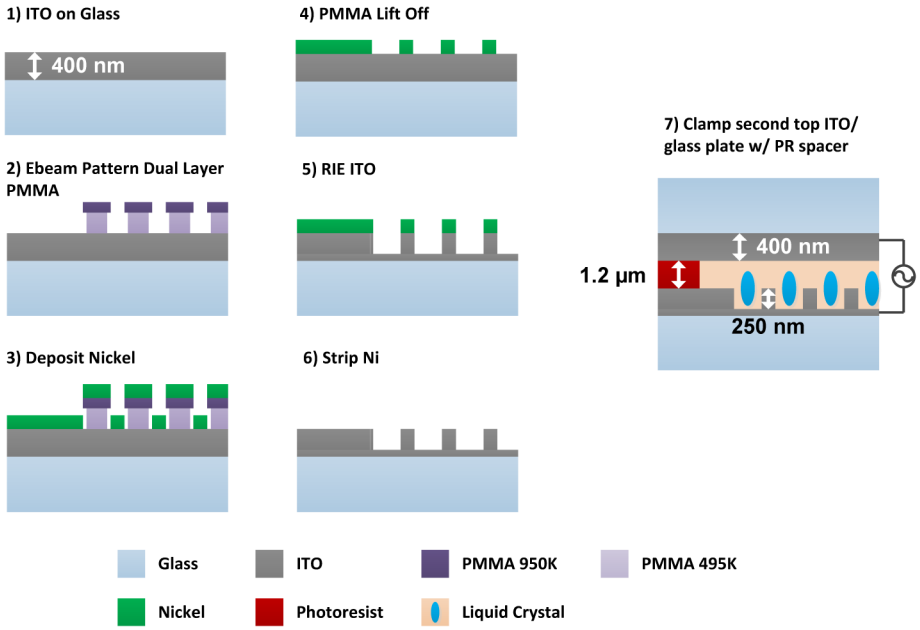

Fig. 4. Fabrication process flow of the ITO etched CDW liquid crystal cell.

The geometry of the patterns consists of segmented ridges of ITO, which approximate the shape of a cycloid and are intended to guide the alignment of the liquid crystal molecules. The pixels of this arrangement consist of at least one segment and one adjacent space, while the pitch is defined as the period of the near-cycloid pattern, as shown in Fig. 5(a). The patterning results in device areas of 500 μm × 500 μm, with each area having one pixel size and one period. In order to explore the dependence of optical performance on pixel size and pitch, we fabricate nine combinations of these two parameters, as listed in Fig. 5(a) below. SEM images of the two extreme parameters are shown in Figs. 5(b) and 5(c). All 9 device parameters were fabricated simultaneously on a single substrate. The actual dimensions of the fabricated ridges are smaller than the layout design due to over-etching; this can be especially seen in the 150 nm pixel width shown in Fig. 5(b).

Optics EXPRESS

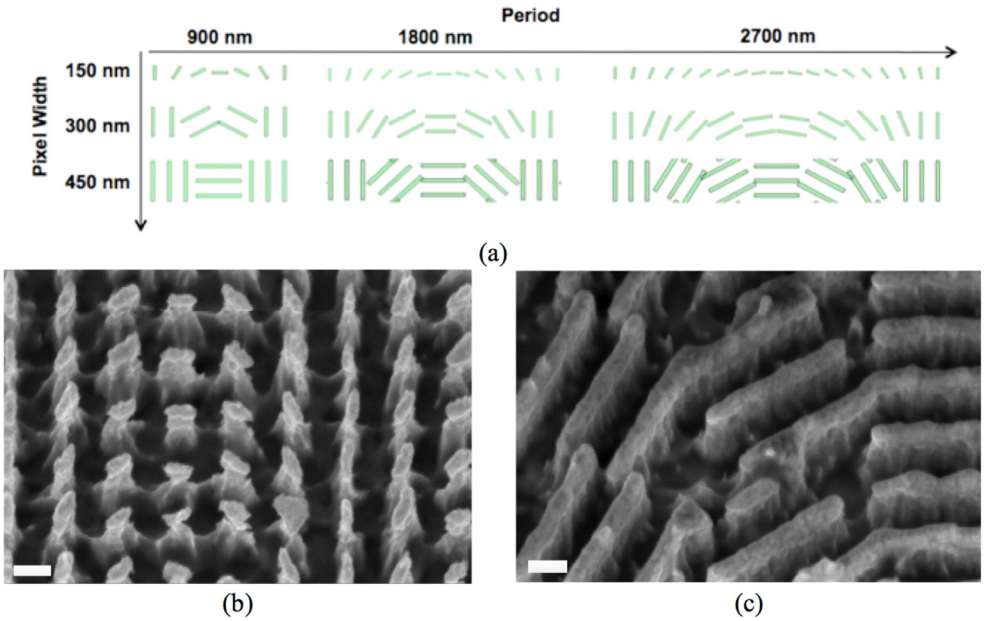

Fig. 5. (a) Schematic of the fabricated pattern variations. SEM image of e-beam defined etched ITO CDW ridges at step 5 in Fig. 4 at a pixel/period length of (b) 150 nm/900 nm and (c) 450 nm/2700 nm. Scale bars are 100 nm.

The optical setup in Fig. 6 was constructed to measure the optical transmission performance of the fabricated CDW liquid crystal cells. A 405 nm wavelength diode laser with a linearly polarized 5 mW output is used as the optical source. A quarter-wave plate designed for 405 nm wavelength is used to circularly polarize the incident beam. When no circular polarization is required, the quarter-wave plate is removed. A telescopic lens system is used to reduce the beam spot size by a factor of 10, accomplished by the ratio of the two focal lengths F_1/F_2. A pin hole with a diameter of 200 μm is located at a distance F_1 away from Lens 1 is used to remove any stray light. The purpose of reducing the beam spot size is to prevent clipping of the input light around the 500 μm × 500 μm e-beam patterned CDW areas. A standard CMOS camera is used to measure the transmitted beam spot profile. The CDW is connected to an AC voltage source with a 1 kHz sinusoidal waveform.

Optics EXPRESS

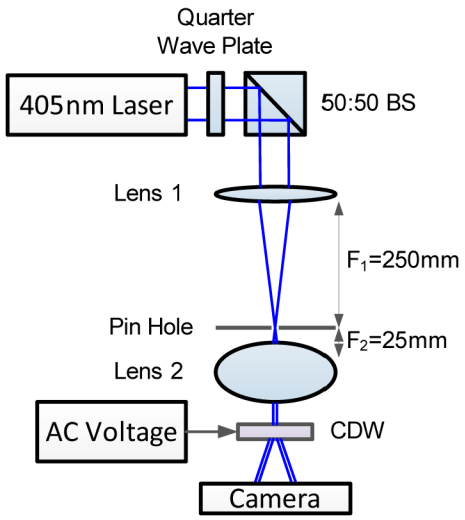

Fig. 6. Schematic of the measurement setup to characterize the CDW performance.

Examples of the measured diffraction results are presented in Fig. 7, where in the "off" state (0 V) the CDW pattern is formed by the guidance of the etched ITO ridges, and thus the non-diffracted M_0 mode is low while the diffracted M_1 is high. In these experiments the input light is not circularly polarized. In the ideal configuration, the "off" state M_0 has zero transmission, but in our experiments it is measurable. This is attributed to two separate causes: (i) the half-wave condition of the cell thickness is not rigorously satisfied, and (ii) the liquid crystal forms a cycloid only through a fraction of the cell thickness, *i.e.*, in the 250-nm-deep gaps between the ITO ridges, as compared to the ~1 μm thickness of the cell. When 10 V is applied to the cell, the CDW pattern is spoiled and the M_0 mode is high while the M_1 is low. In the specific case shown in Fig. 7, the M_0 is increased fourfold and M_1 is decreased fourfold. Thus, in semi-quantitative terms the device behaves as expected for a CDW switchable device.

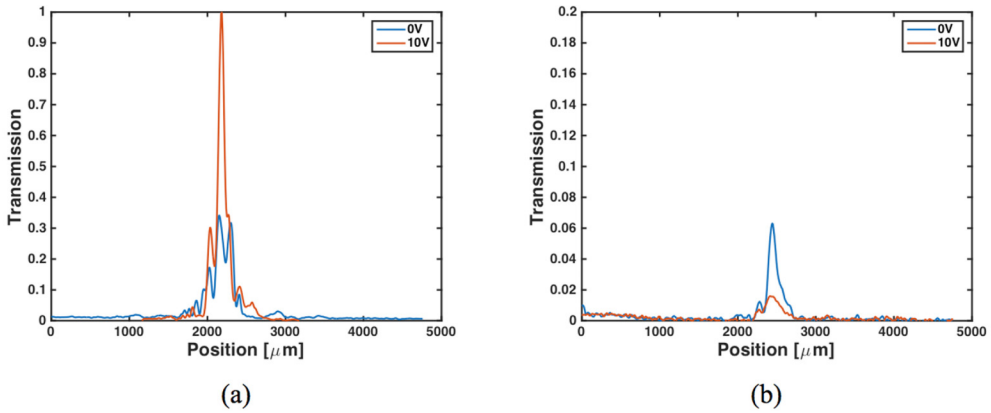

Fig. 7. The measured intensity profile of the (a) M_0 and (b) M_1 mode with a 1kHz sine wave with a peak-to-peak amplitude of 0V and 10V.

The measured efficiencies are shown in Fig. 8 for both DE and PE, at multiple pixel widths and diffraction angles, the latter being defined by the cycloid period. From Fig. 8, the overall DE improves by a factor of up to ~3 with smaller diffraction angles (larger periods), but the diffraction angle has a proportionately smaller effect of ~15% on the PE. These

Optics EXPRESS

observations are consistent with the liquid crystal diffraction efficiency limit trends discussed above and quantified via FDTD simulations, as summarized in Fig. 3. The green curve in Fig. 8 shows the optical performance of the device with no liquid crystal. Due to the index contrast between ITO and the glass substrate, this device is structurally similar to previously demonstrated metasurface designs, however the ITO ridge dimensions were not optimized for an all-dielectric metasurface design and hence the low DE is observed [9–11]. However, the PE for the non-liquid crystal device was similar to the LC device.

The degradation in efficiency of the liquid crystal devices as a function of period is significantly worse than the simulations predicted (black line). In other words, the slope of the simulations (black lines) in Fig. 8 is less steep than the slope of the experimental lines (blue, red, and magenta lines). However, the devices with no liquid crystal (green line) had a slope similar to the FDTD simulations (black line), pointing to the conclusion that the liquid crystal itself is causing the discrepancy. This observation is most likely due to the increased difficulty of maintaining the CDW orientation through the thickness of the cell for smaller periods. The elastic constant of the liquid crystal as well as the anchoring energy of the surface are not taken into account in the FDTD simulation and explain why further degradation is not observed. The experimentally observed effect of diffraction angle on PE is likely due to diffractive effects of the ITO nano-ridges as evidenced by the device with no liquid crystal (green line). Overall, the best experimentally measured DE was 35%, which is significantly lower than the FDTD simulated optimum. On the other hand, the pixel size had a negligible effect on the efficiencies, and any variation between devices with different pixels is within the noise of the measurement. The minimal effect of pixel size, even when the pixel geometry is only a crude approximation of an ideal cycloid, can simplify the required performance of the lithography and fabrication. The devices with periods of 900 nm (26.7°) were also tested but showed no CDW effects and yielded DE = 0 and PE = 0.5.

The overall low efficiencies measured in the fabricated devices can be attributed to the non-ideal assembly process. Primarily, only a single side of the CDW liquid crystal cell contained the etched aligned surface, while the opposing side consisted of unpatterned ITO on a glass substrate. The liquid crystal in contact with the flat surface had no pattern on which to align, and thus the CDW alignment cannot propagate through the entire cell. Furthermore, the flat side was not truly flat as it was composed of an ITO layer, which has a surface roughness about 50 nm in amplitude, measured via an atomic force microscope, which further adds to the misalignment of the liquid crystal. Secondly, although the SU-8 photoresist was used to create the gap spacing, the actual gap can vary quite a bit due to the changing thickness of the SU-8 itself caused by evaporation and liquid crystal diffusion. Additionally, the liquid crystal itself can flow over the SU-8 spacer, further altering the actual gap. Polarized microscope images also revealed significant domain defect lines inside the liquid crystal region, which lead to a slightly opaque appearance of the liquid crystal. Ideally, no defect lines should be present and a clear appearance should be observed [18]. We fully expect that utilizing a more robust liquid crystal cell assembly process and incorporating a dual-sided alignment will significantly increase the overall DE and PE metrics.

Optics EXPRESS

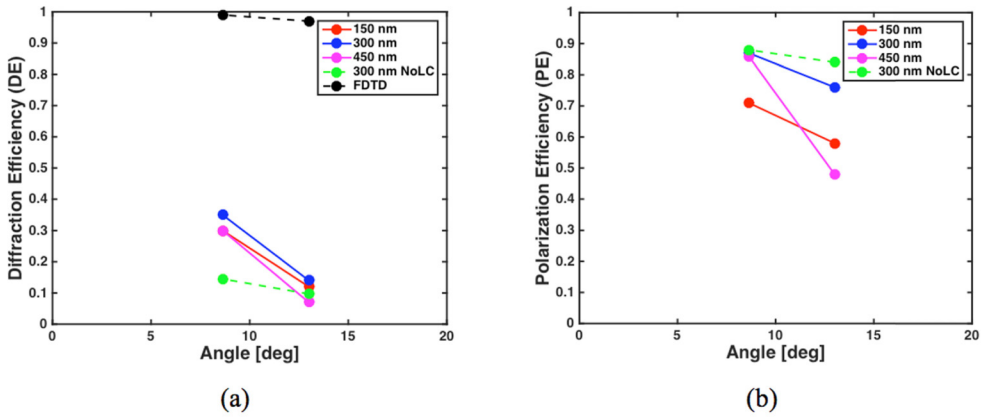

Fig. 8. Measured (a) DE and (b) PE performance of the fabricated CDW liquid crystal cells at 3 different pixel widths of 150 nm, 300 nm, and 450 nm at 0V. The green dashed line is the etched ITO surface only with no liquid crystal and a pixel size of 300 nm. The black dashed line is the FDTD simulated max DE from Fig. 3(a).

4. Conclusion

We successfully demonstrate a fabricated CDW cell using e-beam patterned etched metasurfaces. We demonstrate a peak DE of 35% and a minimum switching voltage of 10 V. We attribute the low efficiencies due to poor assembly process, which can be improved with proper liquid crystal fabrication tools. We also show the simulated theoretical peak efficiencies given an ideal liquid crystal CDW system. Both measurement and simulation show the heavy dependence between increasing DE and decreasing diffraction angle. Unfortunately, the efficiency limit is a fundamental issue with liquid crystal based diffractive waveplates and the index contrast Δn of the liquid crystal. Barring significant improvement in the Δn of a liquid crystal, most diffractive waveplates with high efficiencies are limited to small angles, which sets a limit on the spatial-frequency of advanced diffractive waveplate designs. We note, however, that optical devices that do not rely on the half-wave condition may still benefit from advanced liquid crystal patterns achievable via the flexibility afforded by e-beam patterning, such as alternative tunable metamaterial devices [19].

Funding

This material is based upon work supported by the Department of the Army under Air Force Contract No. FA8721-05-C-0002 and/or FA8702-15-D-0001. Any opinions, findings, conclusions or recommendations expressed in this material are those of the author(s) and do not necessarily reflect the views of the Department of the Army.